# Grb10 regulates the development of fiber number in skeletal muscle

**Lowenna J. Holt,*[,1] Nigel Turner,*[,§] Nancy Mokbel,* Sophie Trefely,* Timo Kanzleiter,* Warren Kaplan,[†] Christopher J. Ormandy,[‡,§] Roger J. Daly,[‡,§,2] and Gregory J. Cooney*[,§,2]**

*Diabetes and Obesity Research Program, [†]Peter Wills Bioinformatics Centre, and [‡]Cancer Research Program, Garvan Institute of Medical Research, Sydney, New South Wales, Australia; and [§]St. Vincent's Hospital Clinical School, University of New South Wales, Sydney, New South Wales, Australia

ABSTRACT **Grb10 is an intracellular adaptor protein that acts as a negative regulator of insulin and insulin-like growth factor 1 (IGF1) receptors. Since global deletion of Grb10 in mice causes hypermuscularity, we have characterized the skeletal muscle physiology underlying this phenotype. Compared to wild-type (WT) controls, adult mice deficient in Grb10 have elevated body mass and muscle mass throughout adulthood, up to 12 mo of age. The muscle enlargement is not due to increased myofiber size, but rather an increase in myofiber number (142% of WT, $P<0.01$). There is no change in myofiber type proportions between WT and Grb10-deficient muscles, nor are the metabolic properties of the muscles altered on Grb10 deletion. Notably, the weight and cross-sectional area of hindlimbs from neonatal mice are increased in Grb10-deficient animals (198 and 137% of WT, respectively, both $P<0.001$). Functional gene signatures for myogenic signaling and proliferation are up-regulated in Grb10-deficient neonatal muscle. Our findings indicate that Grb10 plays a previously unrecognized role in regulating the development of fiber number during murine embryonic growth. In addition, Grb10-ablated muscle from adult mice shows coordinate gene changes that oppose those of muscle wasting pathologies, highlighting Grb10 as a potential therapeutic target for these conditions.—**

**Holt, L. J., Turner, N., Mokbel, N., Trefely, S., Kanzleiter, T., Kaplan, W., Ormandy, C. J., Daly, R. J., Cooney, G. J. Grb10 regulates the development of fiber number in skeletal muscle. *FASEB J.* 26, 3658–3669 (2012). www.fasebj.org**

*Key Words: metabolism · signal transduction · growth factors · proliferation · aging*

Skeletal muscle accounts for 25-40% of body mass, depending on species (1), and up to 85% of postprandial glucose utilization (2). Muscle is also important for fatty acid metabolism and makes a major contribution to total energy expenditure (3, 4). Changes in muscle mass or the ability of muscle to respond appropriately to circulating hormones contribute significantly to metabolic health. In states of obesity, there can be a "spillover" of lipid into inappropriate tissues, particularly skeletal muscle, liver, pancreatic β-cells, and heart (5, 6). In muscle, the accumulation of intramyocellular lipid is associated with insulin resistance and increased risk of type 2 diabetes (7). However, increasing muscle mass by exercise can reduce fat deposition and lipid spillover, thus decreasing metabolic abnormalities. When muscle bulk diminishes, as in aging or disease-related cachexia, insulin resistance is also observed and metabolic health compromised (8). Therefore, investigation into the mechanisms that regulate muscle mass are an important part of understanding whole-body metabolism.

Grb10 is an intracellular adaptor protein that is most highly expressed in insulin-target tissues, such as muscle and adipose tissue, and also in the pancreas (9). It has a multidomain structure and binds to the activated

Abbreviations: β-HAD, β-hydroxyacyl coenzyme A dehydrogenase; BPS, between PH and SH2; CS, citrate synthase; CSA, cross-sectional area; DSHB, Developmental Studies Hybridoma Bank; DXA, dual X-ray absorptiometry; EC, Enzyme Commission; EDL, extensor digitorum longus; EDMD, Emery-Dreifuss muscular dystrophy; FDR, false discovery rate; FGF, fibroblast growth factor; FGFR, fibroblast growth factor receptor; GEO, Gene Expression Omnibus; GSEA, gene set enrichment analysis; H&E, hematoxylin and eosin; HGF, hepatocyte growth factor; IGF1, insulin-like growth factor 1; IGFR, insulin-like growth factor 1 receptor; IR, insulin receptor; IRS-1, insulin receptor substrate 1; MSigDB, Molecular Signatures Database; MyHC, myosin heavy chain; NADH, nicotinamide adenine dinucleotide dehydrogenase; P0, postnatal day 0; PAS, periodic acid Schiff; PCNA, proliferating cell nuclear antigen; PFK, phosphofructokinase; PTTG, pituitary tumor transforming gene; SDH, succinate dehydrogenase; TA, tibialis anterior; WAT, white adipose tissue; WT, wild type

[1] Correspondence: Diabetes and Obesity Research Program, Garvan Institute of Medical Research, 384 Victoria St, Darlinghurst, Sydney, NSW 2010, Australia. E-mail: l.holt@garvan.org.au

[2] These authors contributed equally to this work.

doi: 10.1096/fj.11-199349

This article includes supplemental data. Please visit *http://www.fasebj.org* to obtain this information.



0892-6638/12/0026-3658 © FASEB

insulin receptor (IR; refs. 10–12). Grb10, along with Grb7 and Grb14, belongs to a family of proteins that possess a unique binding region called the between PH and SH2 (BPS) domain (13). This region mediates binding to the IR, along with the SH2 domain, which binds particular phosphorylated tyrosine residues. Resolution of the crystal structure of Grb14-BPS revealed that this region binds and functions as a pseudosubstrate inhibitor of the IR (14). Grb10 can also bind to other growth factor receptors, in which case the SH2 domain is the primary binding module. Evidence exists for interaction of Grb10 with various receptors important in muscle growth. These include the insulin-like growth factor 1 (IGF1) receptor (IGFR), growth hormone receptor (GHR), fibroblast growth factor (FGF) receptor (FGFR), and hepatocyte growth factor (HGF) receptor (cMet) (15–18 and reviewed by Holt and Siddle 19).

Adult mice with a global deletion of Grb10 have an increase in total body weight, accounted for by an increase in lean mass (9, 20, 21). We have previously shown that quadriceps and tibialis anterior (TA) muscles are enlarged in Grb10-disrupted mice (9, 21). In addition, signaling through the IR is enhanced in these muscles, since phosphorylation of insulin receptor substrate 1 (IRS-1) is increased (9). Several studies, from our laboratory and others, have shown that the combined effect of enlarged muscles and enhanced signaling in Grb10-knockout mice is favorable for glucose metabolism (9, 20, 21). However, no studies have yet investigated the physiology underlying this skeletal muscle phenotype.

The metabolic properties of muscle, and its mass, contribute to regulation of whole-body metabolism. Most muscles contain a heterogeneous mix of fibers, depending on their structural, functional, and metabolic requirements (22). Slow-twitch fibers (type I) are highly oxidative and more responsive to insulin, while fast-twitch fibers (type 2B) are more glycolytic and contribute most to muscle bulk and strength (23, 24). The formation of muscle tissue requires a coordinated process involving both hyperplasia during embryogenesis and hypertrophy during postnatal life (25). In the embryo, myoblasts proliferate and differentiate depending on the balance of signals from factors such as IGF1, HGF, FGF, and myostatin (25). These pathways can be manipulated to produce a hypermuscular phenotype. For example, transgenic expression of IGF1 in mice increased muscle mass due to fiber hypertrophy (26, 27). Disruption of myostatin in mice caused a substantial and widespread increase in muscle mass owing to both hyperplasia and hypertrophy (28). While a multitude of studies have also been performed on aspects of myogenesis in cell culture models, the process *in vivo* is highly complex and remains to be fully elucidated.

Here, we report that Grb10-disrupted mice are large and lean throughout life compared to their wild-type (WT) counterparts. Muscle enlargement in 3-mo-old mice is accounted for by increased fiber number in knockout animals. In addition, young mice lacking functional Grb10 are already large by day of birth and have enlarged hindlimbs. Global gene expression profiling revealed up-regulation of functional signatures in neonatal Grb10-knockout mice relating to myogenic signaling and proliferative responses. Taken together, these findings suggest that Grb10 may play a previously unrecognized role in regulating the development of fiber number during murine embryonic growth. In addition, we highlight Grb10 as a potential therapeutic target in states of muscle wasting, since deletion of this adaptor in mice causes gene changes opposed to those seen in cases of muscular dystrophy and muscle inflammation.

## MATERIALS AND METHODS

### Animal maintenance

Animals were kept on a 12-h light-dark cycle with *ad libitum* access to water and standard chow diet. Mice were maintained for roughly 10 generations on a mixed C57BL/6×CBA background. Generation of Grb10-ablated mice has been described previously (29). In brief, the *Grb10* gene was disrupted by deletion of a region spanning exons 2 to 4, thus removing the translation initiation codon from exon 3. *Grb10* is an imprinted gene, and disruption of the maternal allele ablates Grb10 protein expression in skeletal muscle and other peripheral tissues (29). Maternally disrupted heterozygote mice (denoted $Grb10^{m/+}$; also referred to herein as knockout) were used in this study with WT littermates as controls. All studies were carried out on male mice at 3, 6, or 12 mo of age, or neonates at postnatal day 0 (P0) and were undertaken with the approval of the Garvan Institute/St. Vincent's Hospital Animal Ethics Committee, following guidelines issued by the National Health and Medical Research Council of Australia.

### Determination of body composition

Adult or P0 body mass was determined by weighing. Body composition was analyzed by dual X-ray absorptiometry (DXA) using a PIXImus small-animal densitometer and associated software (PIXImus II; GE Medical Systems, Madison, WI, USA). Mice were anesthetized by intraperitoneal injection with ketamine 50 (mg/kg) and xylazine (10 mg/kg). Images were analyzed to give values for lean mass, fat mass, and bone mineral content. Femur length was then determined in Photoshop (given 1 pixel=1.4 mm; Adobe Systems, San Jose, CA, USA). For determination of tissue weights, mice were killed by cervical dislocation; tissues were excised and wet weights were recorded immediately.

### Histology and immunofluorescence

Analysis of P0 hindlimbs was performed by dissecting the limb free between the spine and ankle. Muscles from adult mice were dissected tendon to tendon. Skinned P0 hindlimbs or adult muscles were weighed and then covered with cryopreservation medium (Tissue-Tek; Sakura, Torrance, CA, USA) and frozen in partially thawed isopentane. Transverse cryosections (8 μm) were stained with hematoxylin and eosin (H&E). For immunofluorescence, sections were fixed in ice-cold methanol (50% for 10 min, then 100% for 10 min)

and then blocked in 5% goat serum (Jackson ImmunoResearch Laboratories, West Grove, PA, USA) for 10 min at room temperature (RT). Sections were subsequently incubated at RT for 2 h with dystrophin antibody (1:200; Abcam, Cambridge, UK) to define the sarcolemma for delineating myofiber borders, or antibodies to myosin heavy chain (MyHC) type 1 (1:100; MAB1628; Chemicon-Millipore, Billerica, MA, USA), MyHC type 2A [SC71; Developmental Studies Hybridoma Bank (DSHB), Iowa City, IA, USA] or MyHC type 2B (1:50; BF-F3; DSHB) for fiber-type analysis. After washing with PBS, sections were incubated with secondary antibody, Alexa Fluor 488 goat anti-rabbit IgG or Alexa Fluor 555 goat anti-mouse IgG (both 1:200; Invitrogen Australia, Mt. Waverley, VIC, Australia) for 1 h at room temperature. Samples were mounted with Anti-Fade Fluoromount-G (Southern Biotech, Birmingham, AL, USA). Images were visualized using a Zeiss Axiovert 200 M wide-field fluorescence microscope and captured with AxioVision software (Carl Zeiss, Oberkochen, Germany). For all image analysis, the ImageJ program (U.S. National Institutes of Health, Bethesda, MD, USA) was used. Separate serial sections were also stained for H&E, succinate dehydrogenase [SDH; Enzyme Commission (EC) no. 1.3.5.1], nicotinamide adenine dinucleotide dehydrogenase (NADH; EC 1.6.5.3), or glycogen [periodic acid Schiff (PAS) method] using standard procedures.

#### Enzyme activity measurements

Muscle samples were homogenized 1:19 (w/v) in 50 mM Tris-HCl, 1 mM EDTA, and 0.1% Triton X-100 (pH 7.2), using a Polytron instrument (Kinematica, Littau-Lucerne, Switzerland) and were subjected to 3 freeze-thaw cycles. The activity of phosphofructokinase (PFK; EC 2.7.1.11), β-hydroxyacyl coenzyme A dehydrogenase (β-HAD; EC 1.1.1.35), citrate synthase (CS; EC 4.1.3.7), and SDH was determined at 30°C, as described previously (30) using a Spectra Max 250 microplate spectrophotometer (Molecular Devices, Sunnyvale, CA, USA).

#### Preparation of RNA and gene expression analysis

Total RNA was extracted from frozen hindlimb muscle of neonate (P0) mice or TA muscle of 3-mo-old mice with TRIzol Reagent (Sigma-Aldrich, St. Louis, MO, USA) using standard procedures. The concentration and purity were determined using a NanoDrop spectrophotometer (Biolab, Scoresby, VIC, Australia). RNA quality was assessed using an Agilent 2100 BioAnalyzer (Agilent Technologies, Palo Alto, CA, USA). RNA from either neonate or adult muscle was used on 6 Affymetrix Mouse Gene 1.0 ST microarray chips (Affymetrix, Santa Clara, CA, USA), such that there were 3 chips/genotype (in the case of TA muscle, RNA was taken from pools of 3 animals for each chip so that samples originated from 9 individual animals/genotype). This service was carried out by the Ramaciotti Centre (University of New South Wales, Sydney, NSW, Australia) and included whole-transcript sense labeling with subsequent hybridization to the arrays.

#### Data normalization and statistical analysis

Microarray data analysis was performed using GenePattern (http://www.broadinstitute.org). Normalization and probe set summarization were performed using the robust multi-chip average (RMA) implemented in the Affymetrix library from R/Bioconductor (http://www.bioconductor.org). Differential gene expression between WT and *Grb10*$^{m/+}$ samples was assessed for each probe set using an empirical Bayes moderated *t* statistic, implemented in limma from R/Bioconductor, using the limmaGP tool in GenePattern. *P* values were corrected for multiple hypothesis testing using the positive false discovery rate (FDR). Subsequently, gene set enrichment analysis (GSEA) was performed against the c2_all collection of gene sets from the Molecular Signatures Database (MSigDB; http://www.broadinstitute.org/gsea). Batch effects between neonate and adult data sets were removed using Partek 6.6 software (Partek, St. Louis, MO, USA). The GSEA2EnrichmentMap application (M. J. Cowley, Garvan Institute of Medical Research, unpublished data; a GenePattern tool available from http://pwbc.garvan.unsw.edu.au/gp) was used to filter only the leading-edge genes from each gene set. The data were then uploaded into Cytoscape (http://www.cytoscape.org), and the Enrichment Map plug-in was employed, using the default settings (cutoff values: $P=0.005$, FDR $Q=0.1$, Overlap Coefficient=0.5, and Combined Constant=0.5). For augmenting the c2_all collection with muscle-specific gene sets, the following procedure was used: the Gene Expression Omnibus (GEO; http://www.ncbi.nlm.nih.gov/geo/) was searched for muscle-related data sets. For each data set record, 2 sets of samples were compared by 1-tailed *t* test with a significance level of 0.01 or 0.05 to generate a unique identifier list for up- and down-regulated genes, and the platform was noted. These gene data set (GDS) files and associated platform information were then incorporated into the c2_all collection of gene sets. Genes contained within the best ranking gene sets were then used to identify overlapping pathways with GeneDecks Set Distiller (http://www.genecards.org).

For all other statistical analyses, Student's *t* test was used to determine significant differences between genotypes. For data involving ≥1 age group, Student's *t* test was applied to each age group individually. In addition, 2-way ANOVA with Bonferroni *post hoc* test was used to determine significant differences between genotypes across multiple age groups.

## RESULTS

### Mice with Grb10 disruption are large and lean throughout life

To determine whether increases in body weight and lean mass are maintained throughout the life of *Grb10*$^{m/+}$ mice, body composition was analyzed across 12 mo (**Table 1**). Male mice were used for all studies. *Grb10*$^{m/+}$ male mice exhibited a trend for increased body weight at 3 mo of age and a significant enhancement at 6 and 12 mo of age. The lean mass, measured by DXA, was also significantly increased at these time points. The weights of dissected epididymal and perirenal depots of white adipose tissue (WAT) were decreased significantly for *Grb10*$^{m/+}$ mice at 3 and 6 mo of age. Weights of liver, heart, kidney, and spleen were similar between genotypes at each age examined (data not shown). A small increase in bone mass was observed at each age for *Grb10*$^{m/+}$ mice, which was significant at 12 mo. To investigate whether an increase in skeleton size might contribute to the large body weight of Grb10-deficient mice, nasoanal length, foot length, and femur length were measured (Table 1). Small but significant increases were observed for the first two parameters (ANOVA for effect of genotype, $P<0.05$).

TABLE 1. *Grb10-deficient mice are larger throughout life*

| Parameter | Genotype | Age | | |
|---|---|---|---|---|
| | | 3 mo | 6 mo | 12 mo |
| Body mass (g) | WT | 29.0 ± 0.6 | 31.8 ± 0.7 | 36.1 ± 1.5 |
| | *Grb10*$^{m/+}$ | 31.9 ± 1.5$^{\#}$ | 36.2 ± 1.0*** | 41.0 ± 0.8* |
| Lean mass (g) | WT | 21.4 ± 0.6 | 23.9 ± 0.5 | 24.9 ± 0.6 |
| | *Grb10*$^{m/+}$ | 24.2 ± 1.2* | 27.5 ± 0.7*** | 30.1 ± 0.5*** |
| Fat mass (g) | WT | 4.8 ± 0.3 | 4.7 ± 0.2 | 8.5 ± 1.1 |
| | *Grb10*$^{m/+}$ | 4.8 ± 0.3 | 4.9 ± 0.4 | 7.2 ± 0.6 |
| Bone mass (g) | WT | 0.367 ± 0.013 | 0.364 ± 0.007 | 0.398 ± 0.004 |
| | *Grb10*$^{m/+}$ | 0.408 ± 0.025 | 0.387 ± 0.014 | 0.441 ± 0.016* |
| WAT (g) | | | | |
| Epididymal | WT | 0.63 ± 0.04 | 1.30 ± 0.18 | 0.87 ± 0.09 |
| | *Grb10*$^{m/+}$ | 0.39 ± 0.02*** | 0.64 ± 0.07** | 0.74 ± 0.11 |
| Perirenal | WT | 0.193 ± 0.015 | 0.370 ± 0.048 | 0.394 ± 0.057 |
| | *Grb10*$^{m/+}$ | 0.123 ± 0.018* | 0.201 ± 0.021** | 0.306 ± 0.057 |
| Nasoanal length (cm) | WT | 9.4 ± 0.1 | 9.6 ± 0.1 | 9.8 ± 0.1 |
| | *Grb10*$^{m/+}$ | 9.5 ± 0.2 | 9.9 ± 0.1 | 10.0 ± 0.0 |
| Foot length (cm) | WT | 1.87 ± 0.02 | 1.87 ± 0.02 | 1.87 ± 0.02 |
| | *Grb10*$^{m/+}$ | 1.88 ± 0.03 | 1.92 ± 0.01** | 1.93 ± 0.03 |
| Femur length (cm) | WT | 1.29 ± 0.02 | 1.27 ± 0.03 | 1.36 ± 0.02 |
| | *Grb10*$^{m/+}$ | 1.30 ± 0.01 | 1.33 ± 0.02 | 1.35 ± 0.02 |

Values are expressed as means ± SE; $n$ = 4-12 animals/group. Parameters of body composition were measured for WT and *Grb10*$^{m/+}$ mice in each age group. WAT, white adipose tissue. $^{\#}P = 0.06$, $*P < 0.05$, $**P < 0.01$, $***P < 0.001$ *vs.* WT; Student's t-test.

Taken together, these data demonstrate that the increased body weight of Grb10-deficient mice is maintained throughout life, up to 12 mo of age, and highlight elevated lean mass as the major determining factor.

### Grb10-deficient mice have enlarged muscles

Because lean mass is a large proportion of total body mass and thus has a large effect on whole-body physiology, the muscles of Grb10-deficient mice were examined in detail. Four hindlimb muscles—the extensor digitorum longus (EDL), quadriceps, TA, and soleus—were studied as representatives along the fast-twitch to slow-twitch spectrum. The EDL contains the largest proportion of fast-twitch fibers, while soleus contains the lowest. For each muscle, there was a significant effect of genotype on muscle mass (**Fig. 1**). In the case of EDL, quadriceps, and TA, muscle enlargement was observed in *Grb10*$^{m/+}$ mice at both 6 and 12 mo of age. For soleus, the increase in muscle weight at these ages did not reach significance. Both the EDL and quadriceps showed significant increases in muscle mass for Grb10-deficient mice at 3 mo of age. Taken together, these findings suggest that Grb10-deficient muscles remain larger throughout life and that Grb10 deletion may have a greater effect in the muscles with the higher proportions of type 2 fibers.

### Enlarged muscles of Grb10-deficient mice are due to increased fiber number, with no change in fiber size or fiber type composition

To investigate what accounts for the enlargement of the EDL muscles in Grb10-deficient mice, we analyzed transverse sections through the midbelly region of these muscles from 3-mo-old mice. There was a significant increase in cross-sectional area (CSA) of the total muscle (**Fig. 2*A, B***). To determine whether this was due to an increase in number or size of individual myofibers, quantification was performed. The total number of myofibers in EDL cross sections was significantly elevated for *Grb10*$^{m/+}$ samples (Fig. 2*C*). Similar analysis of the soleus muscle indicated no difference in

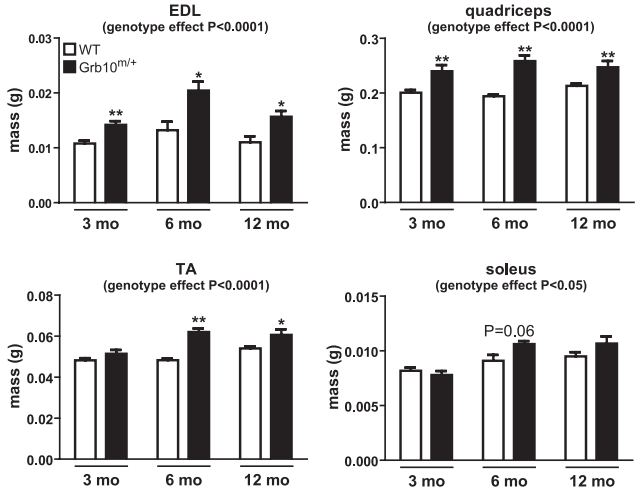


**Figure 1.** Grb10-deficient mice have enlarged muscles. *A*) EDL, quadriceps, TA, and soleus muscles were dissected from WT and *Grb10*$^{m/+}$ mice at 3, 6, and 12 mo of age. Graphs show wet weights. Values are expressed as means ± SE; $n$ = 5–10 animals/group. Comparison of WT and *Grb10*$^{m/+}$ group at each age by Student's $t$ test as indicated; also 2-way ANOVA for genotype and time with significant effect of genotype as indicated ($P<0.0001$ or $P<0.05$). $*P < 0.05$, $**P < 0.01$ vs. WT; Student's $t$ test.

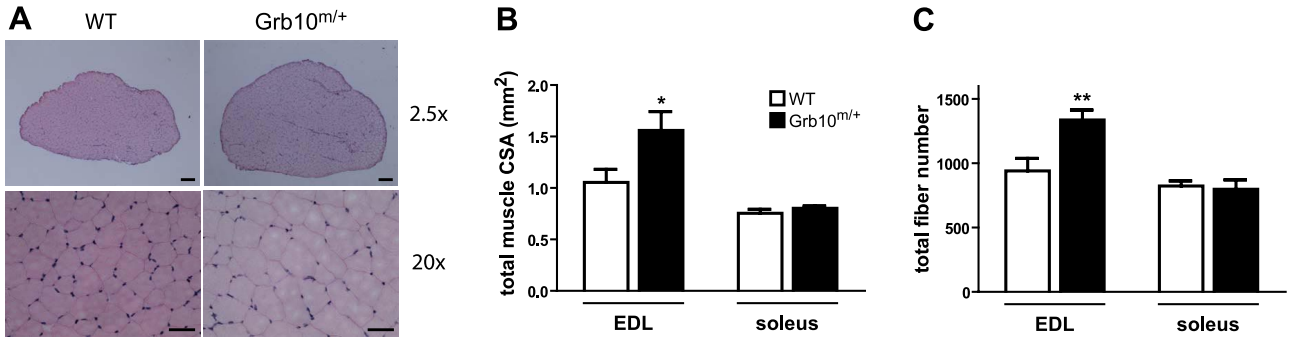


**Figure 2.** Grb10-deficient muscles have more myofibers than their WT counterparts. EDL muscles dissected from 3-mo-old mice were sectioned through the midbelly region. *A*) Representative images of H&E-stained sections to compare WT and *Grb10*$^{m/+}$ EDL total muscle CSA at × 2.5 and general morphology at × 20 view. Scale bars = 200 μm (top panels); 50 μm (bottom panels). *B*, *C*) Total muscle CSA (*B*) and total myofiber number (*C*) for EDL and soleus muscles. Values are expressed as means ± SE; $n = 7$ samples/group. $^*P < 0.05$, $^{**}P < 0.01$ *vs.* WT.

number of individual myofibers or total muscle CSA between genotypes (Fig. 2*B*, *C*). This finding was consistent with the similar mass of WT and *Grb10*$^{m/+}$ soleus muscle from 3-mo-old mice (Fig. 1). For both EDL and soleus, the histomorphology of the muscles was similar between WT and *Grb10*$^{m/+}$ on analysis of transverse sections by H&E staining. Representative images of EDL muscle are shown in Fig. 2*A*. To determine whether fiber sizes were altered in Grb10-deficient muscles, transverse sections were immunostained for MyHC types 1, 2A, and 2B; then individual fibers were measured for CSA. Fibers of the same type were similar in size between WT and *Grb10*$^{m/+}$ samples (**Table 2**). This was the case for fibers from either EDL or soleus muscles.

Because type 1 fibers are smaller than type 2 fibers (31), a significant shift in fiber proportion could also contribute to changes in muscle mass. Therefore, we determined the fiber type proportions in both EDL and soleus muscles from 3-mo-old mice. Type 1, 2A, and 2B fibers were counted and expressed as a percentage of their combined total number in the whole cross section, for EDL or soleus. **Table 3** shows that the proportion of each fiber type was similar for WT and *Grb10*$^{m/+}$ samples. This was the case for EDL and soleus muscles. In addition, visual inspection revealed that the general mosaic distribution pattern of different fiber types was similar between WT and *Grb10*$^{m/+}$ sections for both muscles and that fibers of the same type appear similar between WT and *Grb10*$^{m/+}$ samples (EDL shown as example in **Fig. 3**, top panel). Taken together, these data indicate that elevated fiber number, rather than any change in fiber size or composition, underlies the increased mass of *Grb10*$^{m/+}$ EDL muscle.

Other tissues with significant expression of Grb10 showed an increase in size (pancreas) or decrease in size (adipose tissue) in the adult *Grb10*$^{m/+}$mice. Preliminary investigations determined that there was no difference in the number and size of cells per unit area in pancreas of WT or *Grb10*$^{m/+}$mice (islet cells: WT 1.43±0.23, knockout 1.43±0.17 cells/unit$^2$; nonislet cells: WT 0.51±0.06, knockout 0.52±0.04 cells/unit$^2$) and that the decreased size of adipose tissue in *Grb10*$^{m/+}$mice is associated with a marked reduction in adipocyte size (WT 137±23, knockout 50±15 pL, $P<0.05$).

Substrate metabolism in muscles affects whole-body

TABLE 2. *Fibers of the same type, in EDL or soleus muscle, are similar in size for WT and Grb10-deficient mice*

| Muscle and fiber type | Fiber size (μm$^2$) | |
|---|---|---|
| | WT | *Grb10*$^{m/+}$ |
| EDL | | |
| 1 | 244 ± 34 | 235 ± 37 |
| 2A | 252 ± 21 | 245 ± 20 |
| 2B | 884 ± 103 | 807 ± 79 |
| Soleus | | |
| 1 | 735 ± 12 | 793 ± 79 |
| 2A | 699 ± 53 | 781 ± 108 |
| 2B | NP | NP |

Values are expressed as means ± SE. Myofiber CSA was measured for EDL and soleus from 3-mo-old WT and *Grb10*$^{m/+}$ mice. For EDL, $n = 4$ mice for WT and *Grb10*$^{m/+}$. For soleus, $n = 3$ mice for WT and 4 mice for *Grb10*$^{m/+}$. No significant difference was observed in each case. NP, not present.

TABLE 3. *Fiber type composition, in EDL or soleus muscle, is similar for WT and Grb10-deficient mice*

| Muscle and fiber type | Percentage | |
|---|---|---|
| | WT | *Grb10*$^{m/+}$ |
| EDL | | |
| 1 | 13 ± 2 | 13 ± 1 |
| 2A | 16 ± 3 | 16 ± 2 |
| 2B | 71 ± 4 | 71 ± 4 |
| Soleus | | |
| 1 | 35 ± 2 | 37 ± 3 |
| 2A | 64 ± 2 | 61 ± 2 |
| 2B | 1 ± 1 | 2 ± 1 |

Values are expressed as means ± SE. Fiber types were identified by MyHC immunoreactivity, and then fibers were counted and expressed as a percentage of total type 1, 2A, and 2B fibers in the whole cross section. For EDL, $n = 4$ mice for WT and *Grb10*$^{m/+}$. For soleus, $n = 3$ mice for WT and 4 mice for *Grb10*$^{m/+}$. No significant difference was observed between genotypes.

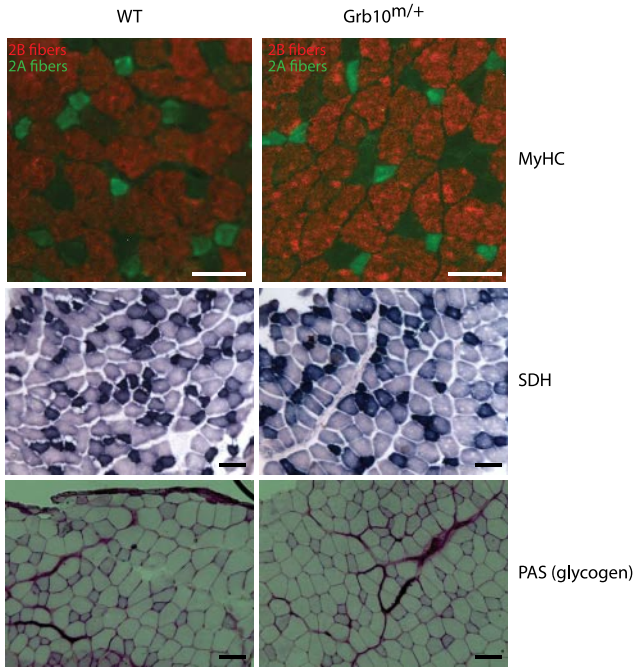


**Figure 3.** Grb10-deficient muscles are not altered in fiber size, fiber proportions, or metabolic properties. EDL muscles dissected from 3-mo-old mice were sectioned through the midbelly region; representative images are shown. Top panel: immunofluorescence for type 2A and 2B fibers. Middle panel: SDH stain. Bottom panel: PAS stain for glycogen. Scale bars = 50 μm.

energy homeostasis. Therefore, we examined the oxidative capacity of WT and *Grb10*$^{m/+}$ muscles. Transverse sections of EDL were stained for the mitochondrial enzymes SDH and NADH reductase. A representative image of the SDH stain is shown in Fig. 3 (middle panel). A similar staining pattern and intensity were observed between WT and *Grb10*$^{m/+}$ samples for both SDH and NADH reductase stains. The glycogen storage in EDL muscle was also assessed by staining transverse sections using the PAS method (Fig. 3, bottom panel). No difference in glycogen content was observed between WT and *Grb10*$^{m/+}$ samples. Similar results were also obtained from analysis of soleus, quadriceps, and TA muscles (data not shown). For a quantitative assessment of muscle metabolic properties, we additionally performed enzyme activity assays. As expected, higher oxidative capacity was observed for soleus muscle compared to EDL (**Table 4**). Comparison of WT and *Grb10*$^{m/+}$ samples indicated no difference in enzyme activities from the glycolytic pathway (PFK) or oxidative pathways (β-HAD, CS, SDH) for either EDL or soleus muscle.

### Grb10-deficient mice are already large by day of birth

Because fiber number is essentially established by day of birth (32), we examined newborn mice at P0. Consistent with the findings of Charalambous *et al.* (29), Grb10-deficient neonates had greater total body mass than WT littermates (**Fig. 4*A***). To investigate whether the muscles were larger in Grb10-deficient neonates, hindlimbs were dissected for further analysis. It was found that hindlimbs from *Grb10*$^{m/+}$ mice were ~2-fold larger than those from WT mice (198±23%; Fig. 4*B*). Since the hindlimbs predominantly comprise both muscle and bone, sections of hindlimb were stained with H&E to delineate these structures. Analysis of the CSA of both the tibia and the fibula bones revealed no size difference between genotypes (data not shown), while the CSA of the total hindlimb was significantly enlarged for Grb10-deficient mice (137±5% of WT; Fig. 4*C*, *D*). Taken together, these data suggest that the hindlimb muscle mass of Grb10-deficient mice is already enlarged by day of birth.

### Effect of Grb10 ablation on gene expression in developing and mature muscles

To investigate the effect of Grb10 deletion on gene expression in muscle, Affymetrix arrays were employed. Independent experiments were performed to compare WT and *Grb10*$^{m/+}$ muscle from either newborn mice (P0, hindlimb) or adult mice (3 mo old, TA). In both cases, the most significant (*Q*) gene change was *Grb10* itself, being down-regulated in *Grb10*$^{m/+}$ samples (Supplemental Tables S1*B* and S2*B*). The most up-regulated genes were *MYH4* (the gene for MyHC 2B) for neonate muscle and *triadin* for adult muscle (Supplemental Tables S1*A* and S2*A*). To identify further functional consequences of the loss of Grb10, GSEA was employed using the c2_all collection of MSigDB gene sets and an additional 63 muscle-specific gene sets generated from GEO. GSEA identifies patterns of gene expression that are empirically associated with function. It was notable that in neonate muscle, the majority of gene sets were positively enriched (the expression pattern was in-

TABLE 4. *No major alterations in metabolic properties of Grb10-disrupted muscles*

| | | EDL | | Soleus | |
|---|---|---|---|---|---|
| Pathway | Enzyme | WT | *Grb10*$^{m/+}$ | WT | *Grb10*$^{m/+}$ |
| Glycolytic | PFK | 328 ± 50 | 387 ± 35 | 128 ± 28 | 202 ± 45 |
| Oxidative | β-HAD | 23.7 ± 1.0 | 23.5 ± 1.1 | 80.5 ± 3.2 | 82.3 ± 2.5 |
| | CS | 307 ± 16 | 299 ± 9 | 515 ± 22 | 548 ± 13 |
| | SDH | 7.6 ± 0.4 | 7.3 ± 0.3 | 13.3 ± 0.2 | 13.9 ± 0.5 |

Values are expressed as means ± SE; $n$ = 9–10 animals/genotype. Enzyme activities (nmol/min/mg protein) in muscle homogenates from WT and *Grb10*$^{m/+}$ mice. No significant difference was observed between genotypes.

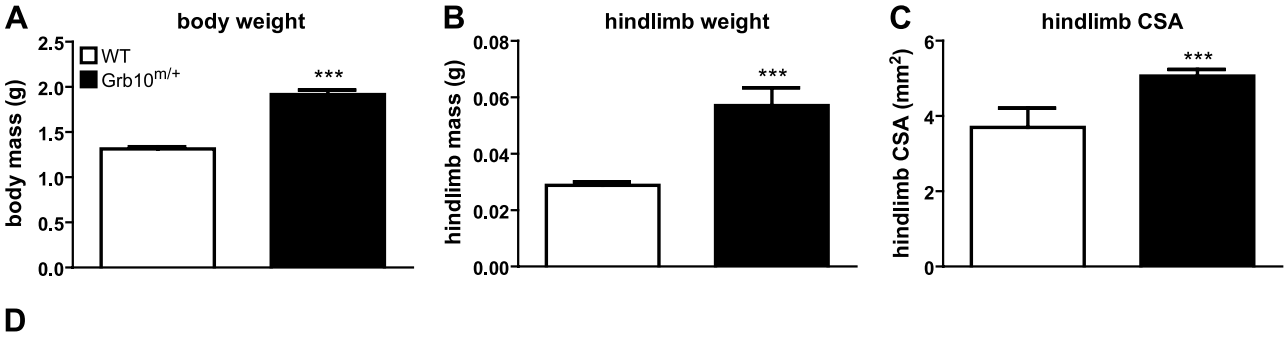


**Figure 4.** Grb10-deficient mice are already large by day of birth. *A*) WT and *Grb10*$^{m/+}$ neonate pups (P0) were analyzed for body weight. *B, C*) Hindlimbs were dissected and measured for weight (*B*) and CSA (*C*). *D*) Representative image for H&E stain of section through the neonate hindlimb. T, tibia; F, fibula. Values are expressed as means ± SE; $n$ = 4-8 (WT) and 3-10 (*Grb10*$^{m/+}$) animals. Scale bars = 200 μm. ***$P < 0.001$ *vs.* WT.

duced) in knockout mice (2291/2551), whereas in adult muscle, the opposite was observed.

The neonate and adult muscle data were examined using Cytoscape, running the Enrichment Map plug-in, to visualize the functional consequences of loss of Grb10 (**Fig. 5** and Supplemental Fig. S5 for scalable version, including gene set names). Gene sets are visualized as nodes, with the outer ring of color representing enrichment in neonate muscle and the center color representing enrichment in the adult muscle. Positively enriched genes sets are red, negatively enriched are blue, and unenriched are white, with greater depth of color indicating more significant enrichment. Overlap of the leading edge genes between nodes is indicated by a green line, with thickness indicating the number of overlapping genes within the two sets. Node size is proportional to gene set size. Three common patterns are observed: sets induced in neonate and adult knockout (nodes all red), those that are induced in neonate knockout and suppressed in the adult

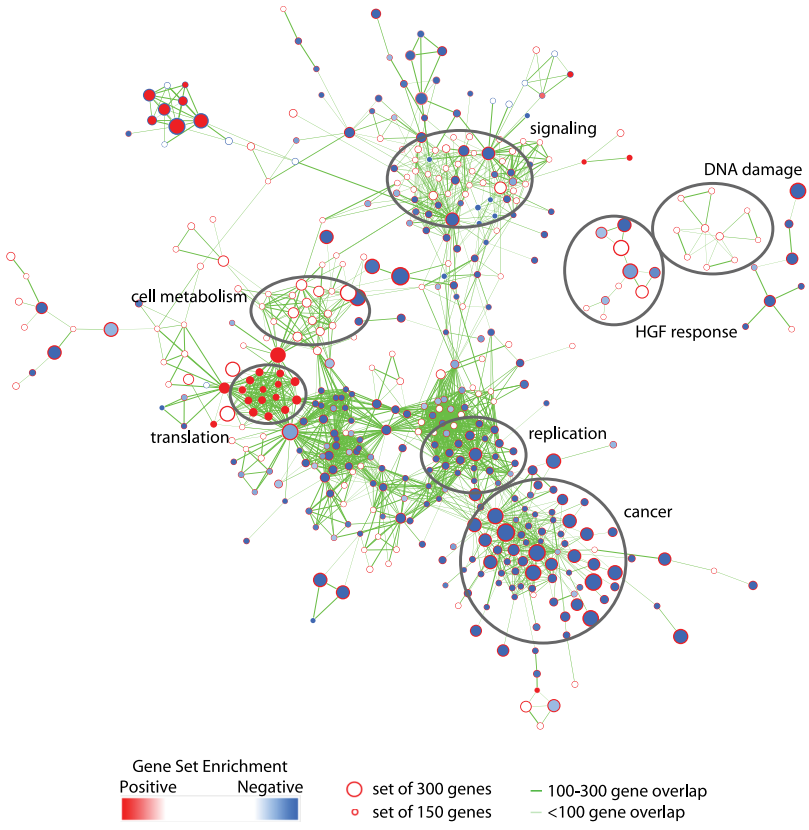


**Figure 5.** Visualization of changes in functional gene signatures between WT and Grb10-deficient mice for muscle from neonate and adult animals. GSEA identified signatures indicative of function within expression profiles derived from Grb10-ablated muscle in neonate (P0) and adult (3 mo old) mice. Data were visualized using the Enrichment Map plug-in for Cytoscape. Each gene set is represented by a circular node. Diameter indicates size; outer ring of color represents the magnitude and direction of enrichment (see scale) in neonate muscle; fill color indicates enrichment in adult muscle. Thickness of the edges (green lines) is proportional to the similarity of linked nodes. The most related clusters are located closest to each other.

knockout (red ring, blue fill), and those that show induction in the neonate knockout but no change in adult knockout (red ring, white fill). The gene sets have been broadly categorized into clusters as shown in Fig. 5. For example, the translation cluster is induced in Grb10-deleted muscle from both neonate and adult mice. The signaling cluster (*e.g.*, RAS, ERK, MAPK, and PI3K pathway gene sets, shown in Supplemental Fig. S5) is induced in neonate knockout muscle but shows mostly no difference between WT and knockout for adult muscle. The same is true for the DNA damage and cell metabolism clusters. The third major category of clusters contains gene sets that show opposite behavior in neonate *vs.* adult (in this case, induced in neonate knockout, suppressed in adult knockout). Notably, these large clusters contain gene sets relating to cancer and replication, and are populated by proliferation-related genes.

In relation to the role of Grb10 as a regulator of cell signaling, the signaling cluster was interrogated to reveal common genes underlying this network. These include genes such as *Akt1*, *Stat3*, *Gab1*, *Raf1*, and *TGF*β (data not shown). In addition, to gain insight into which myogenic signaling pathways might be most affected by Grb10 deletion, a list of growth factor-related gene sets was compiled (**Table 5**). The best ranking gene sets up-regulated in *Grb10*$^{m/+}$ neonate muscle included those for IGF1 signaling and HGF/cMet signaling. To understand the mechanism by which Grb10 deletion may be affecting the development of fiber number, we interrogated the cancer and replication clusters and found that genes such as *Ki67*, proliferating cell nuclear antigen (*PCNA*), and pituitary tumor transforming gene 1 (*PTTG1*) were up-regulated in neonate knockout muscle, but down-regulated in adult knockout muscle.

To further investigate changes in mature Grb10-ablated muscle, additional analyses were performed using GSEA on the corresponding transcript profiling data set, and a list of the muscle-specific gene sets were compiled (**Table 6**). The most enriched gene sets consisted of those relating to muscular dystrophy or inflammation, and for the most part, changes in gene expression occurred in the opposite direction following Grb10 ablation (8/11 and 3/5, respectively). The leading edge genes were used to identify pathways in common using GeneDecks. This analysis revealed that genes from each set were involved not only in general cellular processes like mortality/aging, homeostasis/metabolism, and growth/size, but also more specifically in signal transduction and ubiquitin-related pathways (**Fig. 6** and Supplemental Table S3).

## DISCUSSION

Mice deficient for Grb10 are large and hypermuscular, but the physiology and mechanisms underlying this phenotype have not previously been investigated. In this study, we sought to characterize the muscle enlargement of Grb10-ablated mice and examined changes in gene expression that might contribute to the observed phenotype. We report that muscles from Grb10-knockout mice are composed of more fibers compared to WT, thus implicating Grb10 in playing a role during embryonic muscle development. Analysis of gene expression profiles in neonatal muscle from Grb10 knockout mice revealed up-regulation of proliferative/cancer gene clusters and signaling pathways involved in myogenesis as possible mechanisms for the differences in knockout muscle.

It is interesting to compare *Grb10*$^{m/+}$ mice with other models of hypermuscularity. Transgenic expression of IGF1 (27) or constitutively active Akt (33), and models disrupting the myostatin pathway [*e.g.*, *myostatin*$^{-/-}$ (28), *c-ski* Tg (34), *follistatin* Tg and *ActRIIB*-dominant negative (35)], have muscles increased in size by ~2-fold. All of these models display fiber hypertrophy (with or without parallel hyperplasia). By comparison, the *Grb10*$^{m/+}$ phenotype is modest. At 3 mo of age, we found no evidence of fiber hypertrophy in EDL muscle (even though this muscle was enlarged 32%

TABLE 5. *Enriched gene sets relating to myogenic growth factor pathways, with their rank for expression in neonate Grb10*$^{m/+}$ *muscle*

| Pathway | Gene set name | Rank | *P* | NES |
|---|---|---|---|---|
| | Up-regulated in neonate *Grb10*$^{m/+}$ muscle | | | |
| IGF1 | KUNINGER_IGF1_VS_PDGFB_TARGETS_UP | 510 | <0.0001 | 2.184 |
| FGF | None | | | |
| HGF/cMet | SEIDEN_ONCOGENESIS_BY_MET | 96 | <0.0001 | 2.714 |
| | RUTELLA_RESPONSE_TO_HGF_UP | 132 | <0.0001 | 2.625 |
| | RUTELLA_RESPONSE_TO_HGF_VS_CSF2RB_AND_IL4_UP | 178 | <0.0001 | 2.547 |
| | RUTELLA_RESPONSE_TO_HGF_VS_CSF2RB_AND_IL4_DN | 314 | <0.0001 | 2.355 |
| | Down-regulated in neonate *Grb10*$^{m/+}$ muscle | | | |
| IGF1 | None | | | |
| FGF | REACTOME_FGFR_LIGAND_BINDING_AND_ACTIVATION | 95 | <0.0001 | −1.333 |
| | REACTOME_DOWNSTREAM_SIGNALING_OF_ACTIVATED_FGFR | 197 | <0.0001 | −0.963 |
| HGF/cMet | XU_HGF_TARGETS_REPRESSED_BY_AKT1_DN | 257 | <0.0001 | −0.736 |

GSEA data from neonate muscle were searched for gene sets containing the words IGF, FGF, HGF, or Met. Nominal *P* values are shown. NES, normalized enrichment score.

TABLE 6. *Top-ranking muscle-specific gene sets from GSEA of adult array data*

| Rank | Muscle-specific gene data set for genes up-regulated or down-regulated in *Grb10*$^{m/+}$ muscle | *P* |
|---|---|---|
| | Up-regulated | |
| 330 | GDS2855_DOWN_IN_EDMD_500-764 | 0.9310 |
| 338 | GDS3209_DOWN_IN_INTEGRIN-A7 | 0.7222 |
| 369 | GDS3475_DOWN_IN_LGMD | 0.8421 |
| | Down-regulated | |
| 9 | GDS2855_UP_IN_EDMD | <0.0001 |
| 18 | GDS3463_UP_IN_SEPSIS_500-999 | <0.0001 |
| 39 | GDS3463_UP_IN_SEPSIS_1000-1499 | <0.0001 |
| 59 | GDS3290_DOWN_IN_IL6INFUSED | <0.0001 |
| 75 | GDS2855_DOWN_IN_FKRP_MUT | <0.0001 |
| 94 | GDS2855_UP_IN_DUCHENNEMD_500-999 | <0.0001 |
| 131 | GDS2855_UP_IN_DUCHENNEMD_1-499 | <0.0001 |
| 169 | GDS3475_UP_IN_LGMD | <0.0001 |
| 178 | GDS3474_UP_IN_LGMD | <0.0001 |
| 180 | GDS3027_DOWN_IN_DUCHENNE_MD_1-499 | <0.0001 |
| 214 | GDS3463_UP_IN_SEPSIS_1-499 | <0.0001 |
| 228 | GDS3463_DOWN_IN_SEPSIS_500-840 | <0.0001 |
| 245 | GDS3027_UP_IN_DUCHENNE_MD_1000-1125 | <0.0001 |
| 278 | GDS2855_UP_IN_BECKER_MD | <0.0001 |
| 292 | GDS2855_UP_IN_DUCHENNEMD_1000-1080 | <0.0001 |
| 320 | GDS2855_DOWN_IN_CALP3_MUT | <0.0001 |
| 330 | GDS278_UP_IN_RESIS_EX | <0.0001 |

The c2_all collection of gene sets from MSigDB was augmented with 63 muscle-specific data sets. GSEA revealed sets that were either up-regulated or down-regulated in adult *Grb10*$^{m/+}$ muscle. Table lists a subset of these, with rank and nominal *P* values.

relative to WT), but there was fiber hyperplasia in *Grb10*$^{m/+}$ mice (~40% increase in fiber number). To our knowledge, this is the first report of mice with hyperplasia without concurrent hypertrophy. The increased muscle mass in *Grb10*$^{m/+}$ mice was also maintained until ≥12 mo of age, which was not the obser-

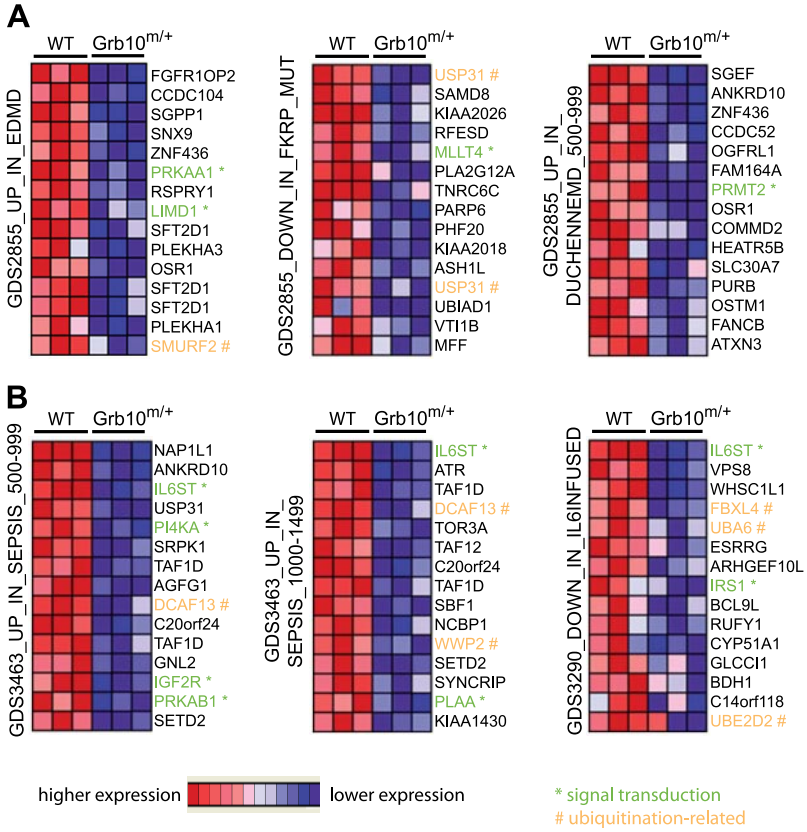


**Figure 6.** Down-regulation of pathology gene sets in Grb10-deficient adult muscle. TA muscle from 3-mo-old mice was analyzed to compare gene expression changes between WT and *Grb10*$^{m/+}$ mice. Top-ranking muscle data sets from GSEA (FDR<25%) revealed linkage to pathologies of muscular dystrophy (*A*), and muscle inflammation (*B*). Heat maps show the expression difference for the top subset of genes in each gene set. Red represents higher expression; blue represents lower expression; $n = 3$/group. Supplemental information on gene descriptions is provided in Supplemental Table S3. Genes common to pathways for signal transduction (*) or ubiquitin-related functions (#) are indicated.

vation with myostatin-null mice (36). Similarly, there is no change in the fiber-type composition of muscles in *Grb10*$^{m/+}$ mice, whereas *myostatin*$^{-/-}$ EDL muscle has a shift away from type 1 and 2A fibers toward type 2B fibers, and, accordingly, a decrease in oxidative enzyme activities (37). These differences between other models of hypermuscularity and *Grb10*$^{m/+}$ mice, coupled with the fact that myostatin-regulated gene sets did not feature in the GSEA of *Grb10*$^{m/+}$ muscle, add evidence for *Grb10*$^{m/+}$ mice being a relatively unique model of increased muscle mass. Thus, the manipulation of Grb10 could be a highly informative and novel avenue for studies exploring the complex process of embryonic myogenesis and, in young adult mice, the effect of hyperplasia without confounding effects of hypertrophy.

Of note, most of our current and published studies only involve male mice. This is mainly because global deletion of Grb10 can lead to a (presumably) developmental complication of imperforate vagina in a considerable number of female mice, which leads to fluid retention in the uterus. However, our initial observations in unaffected knockout females did show the same increase in muscle size observed in male Grb10-deleted mice.

The current study has demonstrated that Grb10-ablated mice have increased myofiber number in EDL muscle compared to WT littermates and that *Grb10*$^{m/+}$ neonate mice have larger hindlimbs than WT counterparts, with an increased CSA. Myogenesis occurs in 2 waves throughout development (E11–E14 and E14–E16), and it is thought that by the time a mouse is born, total myofiber number has been determined (32). In the whole embryo, Grb10 mRNA expression has been shown to peak at E13.5 (38), with strong signals detected in muscle at E13.5, 14.5, 15.5, 16.5, and 18.5 by *in situ* hybridization (29). Taken together, these findings suggest that Grb10 deletion affects the establishment of fiber number during development. It remains to be fully determined why the fiber number of the predominantly white EDL is increased, while that of the predominantly red soleus is unaffected, but one possible explanation is that the temporal expression profile of Grb10 in muscle corresponds more closely with the establishment of secondary myofibers (which will mostly become fast-twitch) rather than that of primary myofibers (which will mostly become slow-twitch).

For a mammal to generate the myofibers ultimately needed by day of birth, a complex and coordinated process of myogenic proliferation and differentiation is required throughout the prenatal period (32). Growth factors essential to this process include IGF1, HGF, and FGF (25). Grb10 binds to receptors for each of these growth factors. For example, stimulation of the IGFR in L6E9 myoblast cultures causes prolonged proliferation (39), and Grb10 has been shown to affect IGF1-mediated proliferation of cultured cells when overexpressed (18, 40). Proliferation of satellite cells from turkeys with enhanced FGF2 signaling is increased (41), and Grb10 does reportedly bind to the FGFR (18). For cMet, disruption of receptor signaling capacity in mice induces a defect in secondary phase myoblast proliferation at E15.5 (42), and Grb10 binds cMet *in vitro* (18). Thus, there is a precedent for an increased proliferative response if any of these Grb10-binding receptors are overstimulated.

GSEA represents a powerful strategy for functional interrogation of global gene transcription patterns. The current analysis shows that the gene expression changes induced by Grb10 deletion are very different in neonate muscle compared to adult muscle. Strikingly, the majority of gene sets was up-regulated in neonate *Grb10*$^{m/+}$ muscle compared to WT, but down-regulated in adult *Grb10*$^{m/+}$ muscle compared to WT. This suggests that many biological pathways in the *Grb10*$^{m/+}$ neonates were subject to a form of negative compensation as the muscle matured. Grb10 is mostly reported as a negative regulator, so it is not surprising that numerous gene clusters were initially up-regulated during development (at P0). Our finding that *Grb10*$^{m/+}$ neonate muscle had an up-regulation of gene clusters relating to cancer and replication are supportive of our hypothesis that deletion of Grb10 affects fiber number during embryogenesis. Of note, in these gene sets were proliferative markers, such as *Ki67* and *PCNA*. Therefore, it is possible that muscle precursor cells undergo enhanced proliferation on Grb10 deletion. Indeed, our work has revealed that genes of the main signaling pathways involved in myogenic proliferation, including IGF1 and HGF/cMet, as well as canonical signaling pathways for proliferation, such as MAPK (ERK and p38) and PI3K, are all up-regulated in *Grb10*$^{m/+}$ neonate muscle. We gained further insight into the signaling pathways that are most likely affected by Grb10 deletion by examining the rank of these pathways in the GSEA output. Notably, HGF/cMet-related gene sets ranked most highly as those up-regulated in *Grb10*$^{m/+}$ neonate muscle. IGF1-related gene sets were less highly ranked, but, notably, there were no matches for the down-regulated gene sets, providing further evidence that IGF1-pathways are also up-regulated in *Grb10*$^{m/+}$ neonate muscle. Future work will be directed toward unraveling the role that Grb10 plays in the complex interaction between myoblast proliferation and differentiation, which ultimately leads to the development of functional myofibers.

Incorporation of additional muscle gene sets into GSEA revealed 2 pathologies that ranked highly in our comparison of WT and *Grb10*$^{m/+}$ muscle in adult mice: muscular dystrophy and muscle inflammation. Muscular dystrophy is characterized by cycles of degeneration and regeneration, but it is ultimately a muscle-wasting disease (43). Similarly the inflammation involved with sepsis causes muscle decline (44). Our finding that the majority of these compromised muscle sets contained genes oppositely regulated to the Grb10-ablated muscle indicates that opposing effects on one or more of the same biological processes may be occurring. Indeed, pathway analysis revealed common groupings of signal transduction and ubiquitin-related functions consistent

with signaling to overall protein breakdown typical of these conditions. Expression of these genes was down-regulated in *Grb10*$^{m/+}$ muscle. For example, interleukin 6 signal transducer (*IL6ST*), a marker of sepsis progression (45), is contained within the "up in sepsis" gene sets but it is down-regulated in Grb10-ablated muscle. It is also interesting to note that Emery-Dreifuss muscular dystrophy (EDMD) affects not only muscle fibers but also satellite cells, likely causing an impaired regenerative response (46). The fact that genes involved in EDMD are down-regulated in *Grb10*$^{m/+}$ muscle supports the hypothesis that Grb10-knockout mice may have enhanced myoblast proliferation and function.

In summary, we have demonstrated that adult mice deficient for Grb10 are hypermuscular because they have more myofibers than WT mice. Newborn mice deficient for Grb10 display up-regulation of functional gene signatures involved in cancer/replication and myogenic signaling. This suggests the novel hypothesis that Grb10 plays a role in regulating the development of fiber number during embryogenesis, by affecting proliferation of muscle precursor cells. We have also shown that the muscular phenotype induced by deletion of Grb10 persists as mice age and revealed that underlying gene changes associated with muscle wasting are oppositely regulated in Grb10-deficient mice. Although further work is required to define the mechanisms in more detail, the structural information available for Grb10 highlights the possibility of investigating this protein as a novel therapeutic target in conditions of muscle wasting. FJ

The authors are grateful to William E. Hughes, Katarina Mele, and James G. Burchfield at the Garvan Institute of Medical Research for helpful discussions regarding the analysis of myofiber morphometry, and Alice Boulghourjian for assistance with H&E stains for histology. The monoclonal antibodies to MyHC-2A (SC-71) and MyHC-2B (BF-F3), developed by S. Schiaffino, were obtained from the Developmental Studies Hybridoma Bank, developed under the auspices of the U.S. National Institute for Child Health and Human Development and maintained by The University of Iowa, Department of Biology (Iowa City, IA, USA). The authors thank Kim Moran-Jones and Tristan J. Iseli at the Garvan Institute for critical reading of the manuscript. The authors also thank the Biological Testing Facility at the Garvan Institute for assistance with animal care. This work was supported by funding from the National Health and Medical Research Council (NHMRC) of Australia (481335). N.T. is supported by a career development award, and C.J.O., G.J.C., and R.J.D. are supported by research fellowships, from the NHMRC of Australia. The authors declare no conflicts of interest.

## REFERENCES

1. Janssen, I., Heymsfield, S. B., Wang, Z., M., and Ross, R. (2000) Skeletal muscle mass and distribution in 468 men and women aged 18-88 yr. *J. Appl. Physiol.* **89,** 81–88
2. DeFronzo, R. A., Jacot, E., Jequier, E., Maeder, E., Wahren, J., and Felber, J. P. (1981) The effect of insulin on the disposal of intravenous glucose. Results from indirect calorimetry and hepatic and femoral venous catheterization. *Diabetes* **30,** 1000–1007
3. Shaw, C. S., Clark, J., and Wagenmakers, A. J. (2010) The effect of exercise and nutrition on intramuscular fat metabolism and insulin sensitivity. *Annu. Rev. Nutr.* **30,** 13–34
4. Lindstedt, S. L., and Conley, K. E. (2001) Human aerobic performance: too much ado about limits to $VO_2$. *J. Exp. Biol.* **204,** 3195–3199
5. McGarry, J. D., and Dobbins, R. L. (1999) Fatty acids, lipotoxicity and insulin secretion. *Diabetologia* **42,** 128–138
6. Kusminski, C. M., Shetty, S., Orci, L., Unger, R. H., and Scherer, P. E. (2009) Diabetes and apoptosis: lipotoxicity. *Apoptosis* **14,** 1484–1495
7. Wells, G. D., Noseworthy, M. D., Hamilton, J., Tarnopolski, M., and Tein, I. (2008) Skeletal muscle metabolic dysfunction in obesity and metabolic syndrome. *Can. J. Neurol. Sci.* **35,** 31–40
8. Evans, W. (1997) Functional and metabolic consequences of sarcopenia. *J. Nutr.* **127,** 998S–1003S
9. Smith, F. M., Holt, L. J., Garfield, A. S., Charalambous, M., Koumanov, F., Perry, M., Bazzani, R., Sheardown, S. A., Hegarty, B. D., Lyons, R. J., Cooney, G. J., Daly, R. J., and Ward, A. (2007) Mice with a disruption of the imprinted Grb10 gene exhibit altered body composition, glucose homeostasis, and insulin signaling during postnatal life. *Mol. Cell. Biol.* **27,** 5871–5886
10. Liu, F., and Roth, R. A. (1995) Grb-IR: a SH2-domain-containing protein that binds to the insulin receptor and inhibits its function. *Proc. Natl. Acad. Sci. U. S. A.* **92,** 10287–10291
11. Hansen, H., Svensson, U., Zhu, J., Laviola, L., Giorgino, F., Wolf, G., Smith, R. J., and Riedel, H. (1996) Interaction between the Grb10 SH2 domain and the insulin receptor carboxyl terminus. *J. Biol. Chem.* **271,** 8882–8886
12. O'Neill, T. J., Rose, D. W., Pillay, T. S., Hotta, K., Olefsky, J. M., and Gustafson, T. A. (1996) Interaction of a GRB-IR splice variant (a human GRB10 homolog) with the insulin and insulin-like growth factor I receptors. Evidence for a role in mitogenic signaling. *J. Biol. Chem.* **271,** 22506–22513
13. He, W., Rose, D. W., Olefsky, J. M., and Gustafson, T. A. (1998) Grb10 interacts differentially with the insulin receptor, insulin-like growth factor I receptor, and epidermal growth factor receptor via the Grb10 Src homology 2 (SH2) domain and a second novel domain located between the pleckstrin homology and SH2 domains. *J. Biol. Chem.* **273,** 6860–6867
14. Depetris, R. S., Hu, J., Gimpelevich, I., Holt, L. J., Daly, R. J., and Hubbard, S. R. (2005) Structural basis for inhibition of the insulin receptor by the adaptor protein Grb14. *Mol. Cell.* **20,** 325–333
15. Morrione, A., Valentinis, B., Li, S., Ooi, J. Y., Margolis, B., and Baserga, R. (1996) Grb10: A new substrate of the insulin-like growth factor I receptor. *Cancer Res.* **56,** 3165–3167
16. Laviola, L., Giorgino, F., Chow, J. C., Baquero, J. A., Hansen, H., Ooi, J., Zhu, J., Riedel, H., and Smith, R. J. (1997) The adapter protein Grb10 associates preferentially with the insulin receptor as compared with the IGF-I receptor in mouse fibroblasts. *J. Clin. Invest.* **99,** 830–837
17. Moutoussamy, S., Renaudie, F., Lago, F., Kelly, P. A., and Finidori, J. (1998) Grb10 identified as a potential regulator of growth hormone (GH) signaling by cloning of GH receptor target proteins. *J. Biol. Chem.* **273,** 15906–15912
18. Wang, J., Dai, H., Yousaf, N., Moussaif, M., Deng, Y., Boufelliga, A., Swamy, O. R., Leone, M. E., and Riedel, H. (1999) Grb10, a positive, stimulatory signaling adapter in platelet-derived growth factor BB-, insulin-like growth factor I-, and insulin-mediated mitogenesis. *Mol. Cell. Biol.* **19,** 6217–6228
19. Holt, L. J., and Siddle, K. (2005) Grb10 and Grb14: enigmatic regulators of insulin action–and more? *Biochem. J.* **388,** 393–406
20. Wang, L., Balas, B., Christ-Roberts, C. Y., Kim, R. Y., Ramos, F. J., Kikani, C. K., Li, C., Deng, C., Reyna, S., Musi, N., Dong, L. Q., DeFronzo, R. A., and Liu, F. (2007) Peripheral disruption of the Grb10 gene enhances insulin signaling and sensitivity in vivo. *Mol. Cell. Biol.* **27,** 6497–6505
21. Holt, L. J., Lyons, R. J., Ryan, A. S., Beale, S. M., Ward, A., Cooney, G. J., and Daly, R. J. (2009) Dual ablation of Grb10 and Grb14 in mice reveals their combined role in regulation of insulin signaling and glucose homeostasis. *Mol. Endocrinol.* **23,** 1406–1414
22. Schiaffino, S. (2010) Fibre types in skeletal muscle: a personal account. *Acta. Physiol. (Oxf.)* **199,** 451–463

23. Gollnick, P. D., Armstrong, R. B., Saubert, C. W., Piehl, K., and Saltin, B. (1972) Enzyme activity and fiber composition in skeletal muscle of untrained and trained men. *J. Appl. Physiol.* **33,** 312–319
24. James, D. E., Jenkins, A. B., and Kraegen, E. W. (1985) Heterogeneity of insulin action in individual muscles *in vivo*: euglycemic clamp studies in rats. *Am. J. Physiol. Endocrinol. Metab.* **248,** E567–E574
25. Velleman, S. G. (2007) Muscle development in the embryo and hatchling. *Poult. Sci.* **86,** 1050–1054
26. Coleman, M. E., DeMayo, F., Yin, K. C., Lee, H. M., Geske, R., Montgomery, C., and Schwartz, R. J. (1995) Myogenic vector expression of insulin-like growth factor I stimulates muscle cell differentiation and myofiber hypertrophy in transgenic mice. *J. Biol. Chem.* **270,** 12109–12116
27. Musaro, A., McCullagh, K., Paul, A., Houghton, L., Dobrowolny, G., Molinaro, M., Barton, E. R., Sweeney, H. L., and Rosenthal, N. (2001) Localized Igf-1 transgene expression sustains hypertrophy and regeneration in senescent skeletal muscle. *Nat. Genet.* **27,** 195–200
28. McPherron, A. C., and Lee, S. J. (1997) Double muscling in cattle due to mutations in the myostatin gene. *Proc. Natl. Acad. Sci. U. S. A.* **94,** 12457–12461
29. Charalambous, M., Smith, F. M., Bennett, W. R., Crew, T. E., Mackenzie, F., and Ward, A. (2003) Disruption of the imprinted Grb10 gene leads to disproportionate overgrowth by an Igf2-independent mechanism. *Proc. Natl. Acad. Sci. U. S. A.* **100,** 8292–8297
30. MacArthur, D. G., Seto, J. T., Chan, S., Quinlan, K. G., Raftery, J. M., Turner, N., Nicholson, M. D., Kee, A. J., Hardeman, E. C., Gunning, P. W., Cooney, G. J., Head, S. I., Yang, N., and North, K. N. (2008) An Actn3 knockout mouse provides mechanistic insights into the association between alpha-actinin-3 deficiency and human athletic performance. *Hum. Mol. Genet.* **17,** 1076–1086
31. Hamalainen, N., and Pette, D. (1993) The histochemical profiles of fast fiber types IIB, IID, and IIA in skeletal muscles of mouse, rat, and rabbit. *J. Histochem. Cytochem.* **41,** 733–743
32. Ontell, M., and Kozeka, K. (1984) Organogenesis of the mouse extensor digitorum longus muscle: a quantitative study. *Am. J. Anat.* **171,** 149–161
33. Lai, K. M., Gonzalez, M., Poueymirou, W. T., Kline, W. O., Na, E., Zlotchenko, E., Stitt, T. N., Economides, A. N., Yancopoulos, G. D., and Glass, D. J. (2004) Conditional activation of akt in adult skeletal muscle induces rapid hypertrophy. *Mol. Cell. Biol.* **24,** 9295–9304
34. Sutrave, P., Kelly, A. M., and Hughes, S. H. (1990) ski can cause selective growth of skeletal muscle in transgenic mice. *Genes Dev.* **4,** 1462–1472
35. Lee, S. J., and McPherron, A. C. (2001) Regulation of myostatin activity and muscle growth. *Proc. Natl. Acad. Sci. U. S. A.* **98,** 9306–9311
36. Elashry, M. I., Otto, A., Matsakas, A., El-Morsy, S. E., and Patel, K. (2009) Morphology and myofiber composition of skeletal musculature of the forelimb in young and aged wild type and myostatin null mice. *Rejuvenation Res.* **12,** 269–281
37. Amthor, H., Macharia, R., Navarrete, R., Schuelke, M., Brown, S. C., Otto, A., Voit, T., Muntoni, F., Vrbova, G., Partridge, T., Zammit, P., Bunger, L., and Patel, K. (2007) Lack of myostatin results in excessive muscle growth but impaired force generation. *Proc. Natl. Acad. Sci. U. S. A.* **104,** 1835–1840
38. Liu, Q., Wang, Y., Chen, Y., Zhang, F. W., Gu, T. T., Qu, Y. P., Yue, L., and Wu, Q. (2009) [The expression analysis of Grb10 during mouse embryonic development]. *Yi Chuan* **31,** 732–740
39. Engert, J. C., Berglund, E. B., and Rosenthal, N. (1996) Proliferation precedes differentiation in IGF-I-stimulated myogenesis. *J. Cell Biol.* **135,** 431–440
40. Morrione, A., Valentinis, B., Resnicoff, M., Xu, S., and Baserga, R. (1997) The role of mGrb10α in insulin-like growth factor I-mediated growth. *J. Biol. Chem.* **272,** 26382–26387
41. Liu, X., McFarland, D. C., Nestor, K. E., and Velleman, S. G. (2003) Expression of fibroblast growth factor 2 and its receptor during skeletal muscle development from turkeys with different growth rates. *Domest. Anim. Endocrinol.* **25,** 215–229
42. Maina, F., Casagranda, F., Audero, E., Simeone, A., Comoglio, P. M., Klein, R., and Ponzetto, C. (1996) Uncoupling of Grb2 from the Met receptor in vivo reveals complex roles in muscle development. *Cell* **87,** 531–542
43. Ruegg, M. A., and Glass, D. J. (2011) Molecular mechanisms and treatment options for muscle wasting diseases. *Annu. Rev. Pharmacol. Toxicol.* **51,** 373–395
44. Callahan, L. A., and Supinski, G. S. (2009) Sepsis-induced myopathy. *Crit. Care Med.* **37,** S354–S367
45. Dougnac, A., Riquelme, A., Calvo, M., Andresen, M., Magedzo, A., Eugenin, E., Marshall, G., and Gutierrez, M. (2001) [Study of cytokines kinetics in severe sepsis and its relationship with mortality and score of organic dysfunction]. *Rev. Med. Chil.* **129,** 347–358
46. Gnocchi, V. F., Ellis, J. A., and Zammit, P. S. (2008) Does satellite cell dysfunction contribute to disease progression in Emery-Dreifuss muscular dystrophy? *Biochem. Soc. Trans.* **36,** 1344–1349

*Received for publication October 31, 2011.*
*Accepted for publication May 8, 2012.*